

PAPER • OPEN ACCESS

Threshold conditions for transversal modes of tunable plasmonic nanolasers shaped as single and twin graphene-covered circular quantum wires

To cite this article: Dariia O Herasymova *et al* 2022 *Nanotechnology* **33** 495001

View the [article online](#) for updates and enhancements.

You may also like

- [Integrated nanolasers via complex engineering of radiationless states](#)
Juan S Totero Gongora and Andrea Fratilocchi
- [Coherent beam combining in optically coupled laser arrays](#)
D.V. Vysotsky and A.P. Napartovich
- [Non-Hermitian gauged topological laser with multi protected modes](#)
Mohammad Mohsen Sheikhey, Arash Dezhang Fard and Hamed Baghban









 **EDINBURGH INSTRUMENTS**

WORLD LEADING MOLECULAR SPECTROSCOPY SOLUTIONS

edinst.com

Threshold conditions for transversal modes of tunable plasmonic nanolasers shaped as single and twin graphene-covered circular quantum wires

Dariia O Herasymova^{1,*} , Sergii V Dukhopelnykov^{1,2} ,
Denys M Natarov¹ , Tatiana L Zinenko¹ , Mario Lucido³  and
Alexander I Nosich¹ 

¹Laboratory of Micro and Nano Optics, Institute of Radio-Physics and Electronics NASU, Kharkiv, Ukraine

²Department of Applied Mathematics, V. N. Karazin Kharkiv National University, Kharkiv, Ukraine

³Department of Electrical and Information Engineering, University of Cassino and Southern Lazio, Cassino, Italy

E-mail: dariia.heras@gmail.com

Received 6 June 2022, revised 18 August 2022

Accepted for publication 30 August 2022

Published 21 September 2022



CrossMark

Abstract

We implement the lasing eigenvalue problem (LEP) approach to study the electromagnetic field in the presence of a circular quantum wire (QW) made of a gain material and wrapped in graphene cover and a dimer of two identical graphene-covered QWs, at the threshold of stationary emission. LEP delivers the mode-specific eigenvalue pairs, namely the frequencies and the threshold values of the QW gain index for the plasmon and the wire modes of such nanolasers. In our analysis, we use quantum Kubo formalism for the graphene conductivity and classical Maxwell boundary-value problem for the field functions. The technique involves the resistive boundary conditions, the separation of variables in the local coordinates, and, for the dimer, the addition theorem for the cylindrical functions. For single-wire plasmonic laser, we derive approximate engineering expressions for the lasing frequencies and threshold values of the gain index that complement the full-wave computations. For the dimer, we derive separate determinantal equations for four different classes of symmetry of the lasing supermodes and solve them numerically. Our investigation of the mode frequencies and thresholds versus the graphene and QW parameters shows that plasmon modes or, for the dimer, plasmon supermodes have lower frequencies and thresholds than the wire modes provided that the QW radius is smaller than $10\ \mu\text{m}$, however in thicker wires they are comparable. Only the plasmon-mode characteristics are well-tunable using the graphene chemical potential. In the dimer, all lasing supermodes form closely located quartets, however, they quickly approach the single-wire case if the inter-wire separation becomes comparable to the radius. These results open a way for building essentially single-mode plasmonic nanolasers and their arrays and suggest certain engineering rules for their design.

Keywords: graphene, quantum wire, eigenvalue problem, lasing, plasmon modes

(Some figures may appear in colour only in the online journal)

* Author to whom any correspondence should be addressed.



Original content from this work may be used under the terms of the [Creative Commons Attribution 4.0 licence](https://creativecommons.org/licenses/by/4.0/). Any further distribution of this work must maintain attribution to the author(s) and the title of the work, journal citation and DOI.

1. Introduction

Graphene is a novel ultra-thin material that has unique electronic and optical properties [1–3]. Today, the patterned graphene shapes such as strips, disks and gratings of them are actively studied in the optical and terahertz wave ranges,

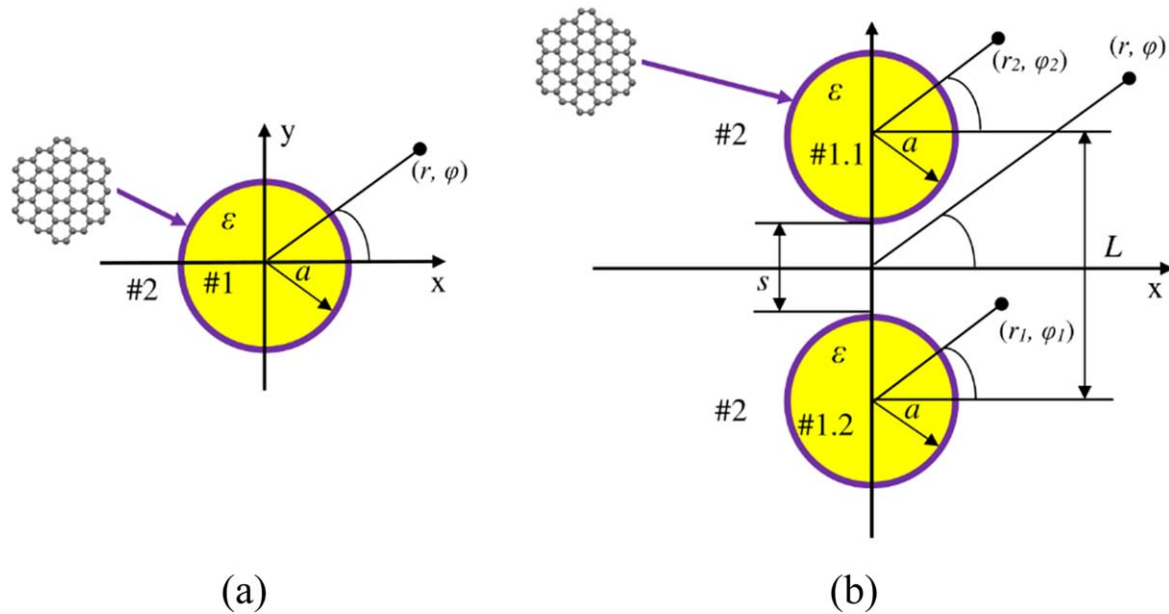


Figure 1. Cross-sectional geometry of a single (a) and a dimer (b) of identical gain-material circular nanowires with graphene covers and the notations used.

where they can be useful as components of novel plasmon waveguides, antennas, sensors and filters [4–8]. This interest is due to the fact that graphene has very good electron conductance, which can be tuned by a DC bias [1–9], that makes the mentioned devices tunable as well. A sheet of graphene is able to support the plasmon guided wave in the infrared and terahertz ranges [2]. On the patterned graphene, such a wave forms the natural plasmon modes (standing waves). Recently, graphene has begun to attract attention as a possible material for the resonant elements of semiconductor plasmonic nanolasers [10, 11] (sometimes, also called spasers; about the terminology, see discussion in [12]). The high cost of the relevant technologies calls for the reliable pre-modeling of the scattering, absorption and emission properties of such devices. Although most frequently graphene is attached to flat dielectric substrates, graphene-covered circular nanowires can be also manufactured; their optical properties have been studied both experimentally [13] and theoretically [14–21].

The goal of our work is to quantify the threshold conditions of the plasmon and other modes of the nanolasers made of a circular QW covered with graphene and a pair of such wires (see figure 1) and investigate their dependences on the QW and graphene parameters. Our instrument is the lasing eigenvalue problem (LEP) approach [22], which has been already applied to several types of microlasers in [23–25] and silver nanostrip and nanotube plasmonic lasers in [26, 27]. LEP is a full-wave semi-classical electromagnetics eigenvalue problem, tailored to extract the mode-specific wavelengths, together with the associated threshold material gain values, of not attenuating in time emission. Complete mathematical grounding of LEP can be found in [28].

Note that the laser configuration in figure 1(a) was considered recently in [21] using essentially a LEP-like approach,

namely, looking for the conditions that turn the imaginary part of the natural frequency of the plasmon mode to zero.

In our work, we build on the conference papers [29, 30], which are considerably extended by adding numerical results and drawing more detailed and grounded conclusions. The remaining part of this work is structured as follows. In section 2, we formulate the considered eigenvalue problems. Sections 3 and 4 deal with characteristic equations and numerical results for the single-wire nanolaser, respectively. Sections 5 and 6 deal with the same issues for the dimer-wire nanolaser. Conclusions are summarized in section 7.

2. LEP statement

As follows from the Poynting theorem, arbitrary *passive* open resonator eigenfrequencies can be only complex, with non-zero imaginary parts that corresponds to finite radiation losses. Therefore, in order to emit electromagnetic wave, which does not attenuate in time, an open resonator must contain an *active zone* filled in with the gain material. In practice, such ‘quantum’ materials can be various semiconductors, dye-doped polymers, or crystalline materials doped with ions of erbium or some other rare-earth elements. All of them are able to demonstrate, under pumping, the inverse population of electronic levels and the stimulated emission of light. Within macroscopic electromagnetics, these properties are translated to the ‘negative losses’ that is expressed by the corresponding sign of the imaginary part of the dielectric constant and refractive index.

Consider a single-wire laser, the active zone of which is a graphene-covered circular QW, as shown in figure 1(a), in the free space. We denote the radius of QW as a and assign the indices 1 and 2 to the inner ($r < a$) and outer ($r > a$) domains of QW, respectively.

We will assume that the wire is infinite along the z -axis and that the electromagnetic field does not depend on z , with time dependence $e^{-i\omega t}$, where the frequency is real, $\omega = \text{Re } \omega$. Thanks to this, we consider a two-dimensional problem in the plane of the wire cross section, where we introduce the polar coordinates, (r, φ) . As graphene is known to support the H -polarized plasmon modes, we consider only this case. Here, the electric and magnetic fields have components $\mathbf{E} = (E_r, E_\varphi, 0)$ and $\mathbf{H} = (0, 0, H_z)$, respectively.

The function $H_z(r, \varphi)$ must satisfy the Helmholtz equation, $(\Delta + k_{1,2}^2)H_z(r, \varphi) = 0$ outside the QW boundary ($r \neq a$), with the wavenumbers $k_1 = k\nu$ and $k_2 = k$, where $k = \omega/c$ and the QW material is nonmagnetic, so that its dielectric constant is connected to the refractive index ν as $\varepsilon = \nu^2$. At the graphene-covered QW boundary, the field function must satisfy the so-called 'resistive' boundary conditions

$$E_\varphi^{\text{int}} = E_\varphi^{\text{ext}}, E_\varphi^{\text{int}} + E_\varphi^{\text{ext}} = 2ZZ_0(H_z^{\text{int}} - H_z^{\text{ext}}), r = a, \quad (1)$$

where Z is the surface impedance of graphene, normalized by the free-space impedance Z_0 ; it has the following form: $Z = (\sigma Z_0)^{-1}$, with σ being the complex surface conductivity. Besides, thanks to real k , the field function must satisfy the Sommerfeld radiation condition at infinity, and, additionally, the condition of the local field power finiteness. Note also that $E_\varphi^{\text{int,ext}} = (Z_0/ik\varepsilon_{1,2})\partial H_z^{\text{int,ext}}/\partial r$, from the Maxwell equations.

We consider the complex refractive index of the QW gain material to be $\nu = \alpha - i\gamma$, where α is known refractive index and $\gamma > 0$ is unknown threshold gain index. We will also assume that the material gain is uniformly distributed throughout the QW and does not depend on the frequency. In real life, such a QW can be a glass-like material doped with erbium ions, to provide the gain in the infrared range. In the sub-THz range, similar properties are found for the andalusite crystalline material doped with iron.

Within the LEP, we look for such pairs of real numbers (k_s, γ_s) that generate non-zero functions $\{\mathbf{E}_s, \mathbf{H}_s\}$ ($s = 1, 2, \dots$), which solve the formulated above boundary-value problem for the Maxwell equations. That is, we look for the frequencies and gain-index thresholds of laser modes as eigenvalue pairs. It is worth to note that the other LEP-like formulations exist, see [31–35], where the threshold gain is characterized with $\text{Im}\varepsilon < 0$ instead of γ or with the product, $g = k\gamma$.

In the dimer case, we introduce the global Cartesian and polar coordinates, with the origins at the midpoint between QW axes so that $\vec{r} = (x, y) = (r, \varphi)$, where $x = r \cos \varphi$, $y = r \sin \varphi$, and two local coordinate systems with the origins at the wire axes (figure 1(b)). Then, the associated LEP formulation is similar to single-wire case, with the conditions (1) imposed at each wire's boundary, $r_j = a$ ($j = 1, 2$). Important circumstance is that the dimer-wire configuration has two lines of symmetry, that is the x and y axes.

Note that, in reality, the gain index of active material depends on the frequency, usually as a bell-like function reaching maximum at a certain central frequency, say, ω_c , and decay parameter, ω_d , which are material specific. To reflect the frequency dispersion of the gain index, one can introduce

the latter quantity into LEP as a function, $\gamma = \bar{\gamma} \exp[-\omega_d^2(\omega - \omega_c)^2]$, and then look for the mode-specific eigenvalue pairs $(k_s, \bar{\gamma}_s)$. Still, even without this modification, LEP enables one to compare various modes by their thresholds.

3. Graphene's conductivity description

The most widely adopted today quantum model of the electron mobility in the graphene monolayer is the Kubo model [2]. Here, the graphene thickness is considered zero, and its surface conductivity, $\sigma(\omega, \mu_c, \tau, T)$ depends on the cyclic frequency ω , chemical potential μ_c , electron relaxation time τ and temperature T . This value consists of two contributions, $\sigma = \sigma_{\text{intra}} + \sigma_{\text{inter}}$, which are intraband and interband conductivities

$$\sigma_{\text{intra}} = \frac{q_e^2 k_B T}{\pi \hbar^2 (1/\tau - i\omega)} \left\{ \frac{\mu_c}{k_B T} + 2 \ln \left[1 + \exp\left(-\frac{\mu_c}{k_B T}\right) \right] \right\}, \quad (2)$$

$$\sigma_{\text{inter}} = \frac{iq_e^2}{4\pi\hbar} \ln \frac{2|\mu_c| - (\omega + i\tau^{-1})\hbar}{2|\mu_c| + (\omega + i\tau^{-1})\hbar}. \quad (3)$$

Then, the normalized (i.e. dimensionless) surface impedance (or resistivity) of graphene is

$$Z(\omega) = Z_0^{-1}(\sigma_{\text{intra}} + \sigma_{\text{inter}})^{-1}. \quad (4)$$

The relative contribution of two terms into (4) depends on the frequency and chemical potential. This can be understood from the curves in figure 2(a) and the color map in figure 2(b).

The interband conductivity, in absolute value, is smaller than the intraband one, which is frequently called the Drude model, in a wide range from the statics to a certain high frequency [2]. The upper bound here scales with the chemical potential, due to the dominance of the term containing the factor $\mu_c(k_B T)^{-1}$ in the Kubo formulas. For instance, if $\tau = 0.5$ ps, $T = 300$ K and $\mu_c = 0.25$ eV, then $|\sigma_{\text{inter}}| \leq 0.1|\sigma_{\text{intra}}|$ at the frequencies below 40 THz, while if $\mu_c = 0.5$ eV, then the same is valid at the frequencies below 80 THz.

Still, above the mentioned frequency, which lays in the near infrared or visible light range, the description of graphene should take into account both types of conductivity. Below, we will use the full expression (4) in the numerical analysis and the simplified description using only the intraband term in the analytical characterization of the plasmon mode frequencies and thresholds.

4. Characteristic equations for the single-wire modes

Consider plasmonic nanolaser on single graphene-covered QW (figure 1(a)). The magnetic field inside and outside the wire can be expanded as Fourier series in the angular exponents, taking into account the radiation condition at infinity and condition of local field power finiteness near the center of

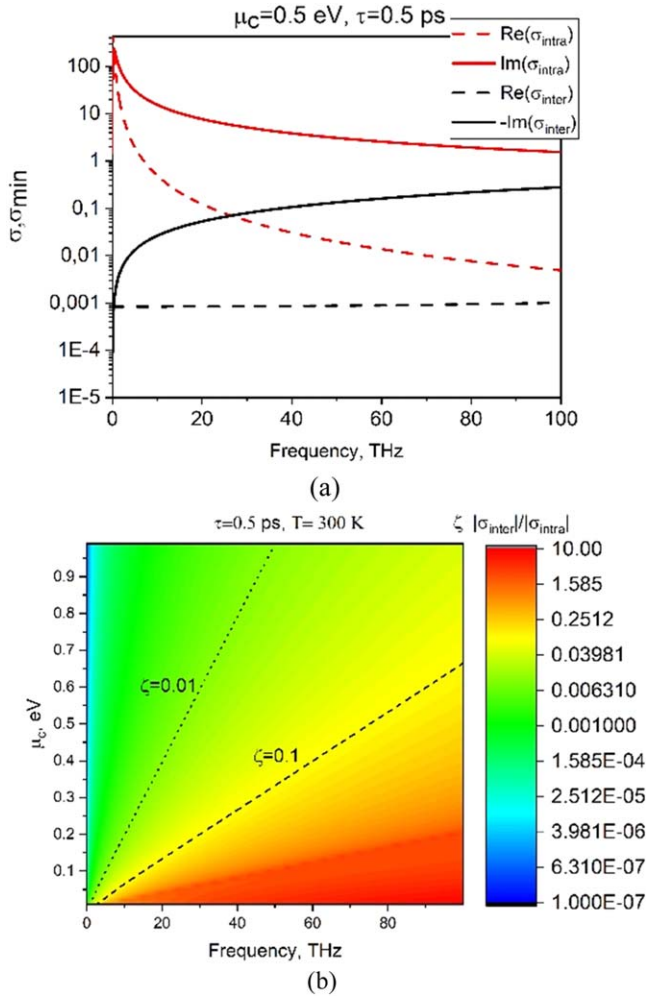


Figure 2. The frequency dependences of the intraband and interband surface conductivities of the monolayer graphene sheet according to the Kubo formalism (a) and the ratio of these two values as a function of the frequency and the chemical potential (b). Electron relaxation time is $\tau = 0.5$ ps, temperature is $T = 300$ K.

wire

$$H_z^{\text{int,ext}}(r, \varphi) = \sum_{m=0(1)}^{\infty} \begin{cases} x_m J_m(\nu kr), & r < a \\ y_m H_m(kr), & r > a \end{cases} \times \cos(m\varphi) \text{ or } \sin(m\varphi), \quad (5)$$

where x_m and y_m are unknown coefficients, while $J_m(\cdot)$ and $H_m(\cdot)$ are the Bessel and the Hankel 1-st kind cylindrical functions, respectively. The orthogonality and completeness of the set of functions $\cos / \sin(m\varphi)$, $m = (0), 1, 2, \dots$ on the circle allow us to apply the conditions (1) in term-by-term manner.

Thus, the separation of variables leads to splitting of the modes into independent orthogonal families by the azimuthal index m , and all modes with $m > 0$ are double degenerate.

After some algebra, independent full-wave transcendental equations for the modes of each index, $m = 0, 1, 2, \dots$, can be written as

$$D_m(k, \gamma; a, \alpha, Z) = J'_m(kva)H'_m(ka) + iZ[J'_m(kva)H_m(ka) - \nu J_m(kva)H'_m(ka)] = 0. \quad (6)$$

Note that if $Z = 0$ or $|Z| \rightarrow \infty$, then, respectively, (6) turns to the characteristic equation for the modes of the circular cavity with PEC wall or the circular dielectric rod in the free space.

We emphasize that the complex calculus theorems guarantee that the roots of (6) are discrete on the plane (k, γ) . Besides, each of them is a continuous function of a , α and Z and cannot appear or disappear on that plane except at $k = 0$ and infinity.

It is interesting that those roots of (6) that correspond to the plasmon modes can be determined analytically, at least in the frequency domain where the intraband conductivity, σ_{intra} , dominates over the interband conductivity, σ_{inter} (see section 3).

In this domain, σ_{inter} can be neglected, and the normalized surface impedance (or resistivity) of graphene takes the following form:

$$Z(\omega) \approx (Z_0 \sigma_{\text{intra}})^{-1} = (1/\tau - i\omega)\Omega^{-1}, \quad (7)$$

$$\Omega = \frac{q_e^2 k_B T Z_0}{\pi \hbar^2} \left\{ \frac{\mu_c}{k_B T} + 2 \ln \left[1 + \exp\left(-\frac{\mu_c}{k_B T}\right) \right] \right\}, \quad (8)$$

where Ω does not depend on the frequency, q_e is the charge of the electron, k_B is the Boltzmann constant, and \hbar is the reduced Planck constant. As one can see, $\text{Im}Z < 0$. Thanks to this, graphene can support the propagation of the plasmon wave [2]. Note that if $\mu_c \gg k_B T$ then the logarithmic term in (8) can be neglected.

Now, we can consider the circular graphene shell as a traveling wave resonator, which supports the transversal plasmon modes (similarly to silver nanotube plasmon modes [36]). Then, neglecting the curvature of the shell, and hence the radiation losses, approximate characteristic equation for these modes is

$$g_{\text{plas}} a = m, \quad m = 1, 2, \dots, \quad (9)$$

where g_{plas} is the propagation constant (eigen-wavenumber) of the plasmon guided wave on the infinite flat graphene monolayer placed between two dielectrics, known in the analytical form from [37]. Namely, if $|Z| \gg 1$, then

$$g_{\text{plas}} \approx ik(\varepsilon + 1)Z + O(1). \quad (10)$$

On substituting (10) and (7) into (9), a complex-valued equation is obtained

$$ika(\varepsilon + 1)Z(k, \gamma) + O(1) = m, \quad m = 1, 2, \dots, \quad (11)$$

which can be solved analytically in the same approximation. Interestingly, the same equation as (11) follows from (6) if $ka \ll 1$ and $|kva| \ll 1$ [21]. The real part of this equation allows to find approximate expression for the frequencies of the transversal plasmon modes of the closed graphene shell

$$k_m^P \approx \left[\frac{m\Omega}{a(\alpha^2 + 1)c} \right]^{1/2}. \quad (12)$$

One can see that in the considered approximation, the frequencies do not depend of the electron relaxation time and are proportional to the square-roots of the chemical potential of graphene (if $\mu_c \gg k_B T$) and inverse QW radius. This opens up the possibility of developing a laser that is continuously tuned in a fairly wide range of frequencies.

Furthermore, the imaginary part of the same equation delivers the threshold values of the gain index

$$\gamma_m^P \approx \frac{(\alpha^2 + 1)^{3/2}}{2\alpha} \left(\frac{a}{m\Omega c} \right)^{1/2} \frac{1}{\tau}. \quad (13)$$

Thus, the lasing thresholds of the plasmon modes are inversely proportional to the electron relaxation time and the square roots of the mode azimuth index and the chemical potential (if $\mu_c \gg k_B T$). Besides, they scale as the square root of the wire radius, although one should keep in mind that (13) is derived neglecting the radiation losses of the plasmons.

Interestingly, frequently used in the laser physics quantity of the product of (12) and (13), which is the gain per wavelength, does not depend on the QW radius, graphene chemical potential and mode index, in the considered approximation, namely

$$k_m^P \cdot \gamma_m^P \approx \frac{\alpha^2 + 1}{2\alpha c \tau} \text{ or } k_m^P \cdot (\text{Im}\varepsilon)_m^P \approx \frac{\text{Re}\varepsilon + 1}{c\tau}. \quad (14)$$

Therefore, within this approximation, all plasmon modes under any variations of these parameters stay at the same hyperbolic trajectory, $k = C(\alpha, \tau) \cdot \gamma^{-1}$, which is controlled only by the electron relaxation time, τ , and wire refractive index, α . This feature is, obviously, the consequence of the fact that the simplified Kubo expression for graphene's surface impedance (7) suggests that both its real and imaginary parts are proportional to $\Omega(\mu_c, T)$, hence their ratio scales as $\omega\tau$.

5. Full-wave analysis of single-wire laser mode properties

In this section, we present the results of numerical study of the LEP eigenpairs for the single-QW graphene-coated laser using the full-wave equation (6) and full Kubo conductivity (2)–(4). In figure 3, the lasing frequencies and thresholds are shown versus the wire radius, which varies from 50 nm to 100 μm , at $\mu_c = 0.25$ eV, $\tau = 0.5$ ps and $\alpha = 1.55$. One can see that the plasmon modes have lower frequencies and thresholds than the first QW modes H_{01} and H_{11} provided that the QW radius is smaller than 10 μm , while in thicker wires they become comparable.

The based on the Drude term approximations (12) and (13) for k_m^P and γ_m^P are also shown by the dotted curves in figure 2. Note that they are in very good agreement with full-wave computations of the roots of (6), performed by the iterative root-search method, where (12) and (13) are the initial-guess values. As expected, the agreement worsens at low frequencies where $|Z|$ gets so small that the radiation

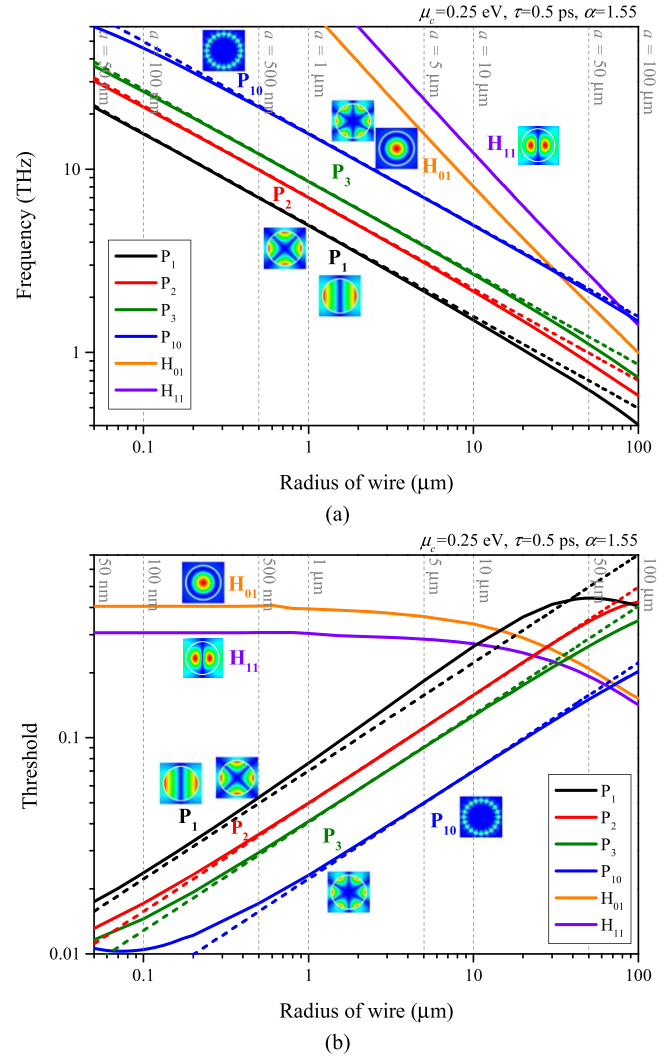
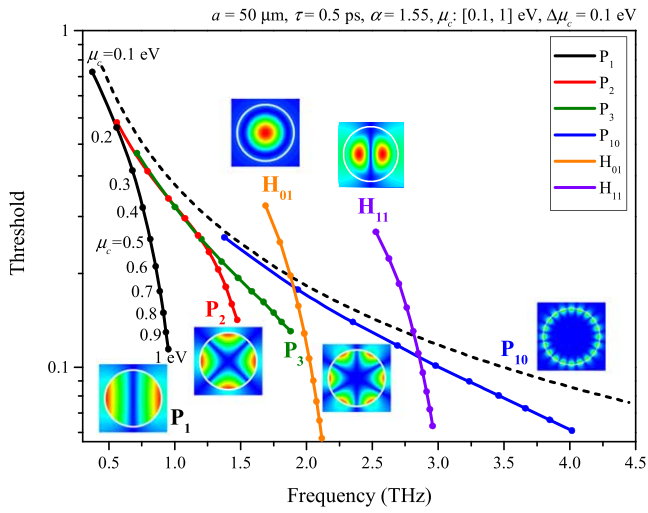


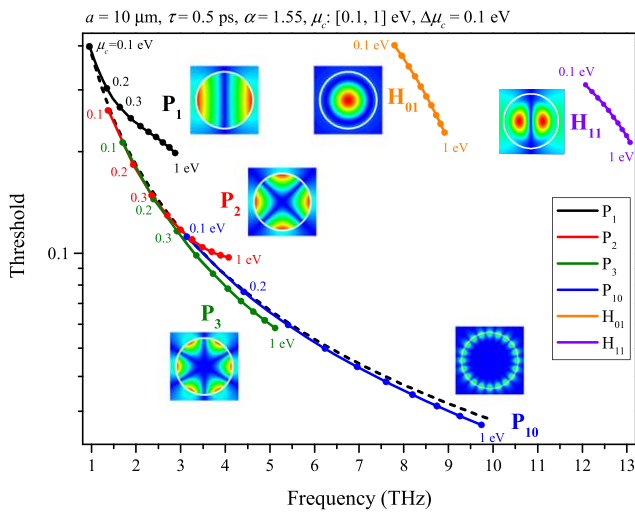
Figure 3. Frequencies and thresholds versus the wire radius a for the plasmon modes P_1 , P_2 , P_3 and P_{10} and the wire modes H_{01} and H_{11} for the single-wire laser with parameters of graphene $\mu_c = 0.25$ eV, $\tau = 0.5$ ps and $\alpha = 1.55$.

losses become comparable to the ohmic losses and at very high frequencies where the contribution of the interband conductivity cannot be neglected.

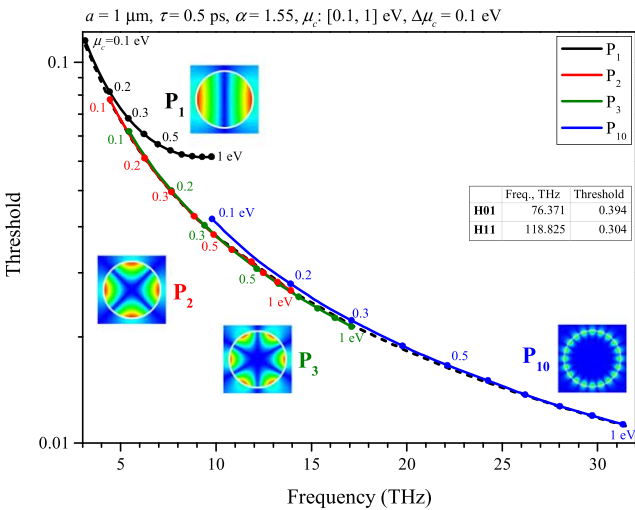
Further, to make clearer the comparison of the lasing conditions, we plot the trajectories of the modes, considered in figure 3, on the plane (f, γ) , where $f = kc/2\pi$, under the variation of the chemical potential of graphene (figure 4), electron relaxation time (figure 5), and QW refractive index (figure 6). Here, we choose the wire radius to be 50 μm , 10 μm and 1 μm and assume that the QW gain material refractive index and the graphene parameters are as indicated in figures. We emphasize that these trajectories have been computed from the full-wave transcendental equation (6) and full Kubo expressions (2)–(4) for several values of the azimuth index m . For comparison, the trajectories based on approximations (12) and (13) are also presented as dashed lines.



(a)

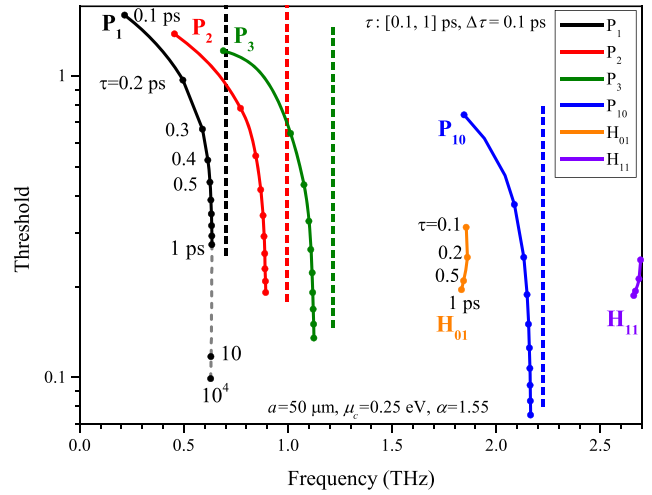


(b)

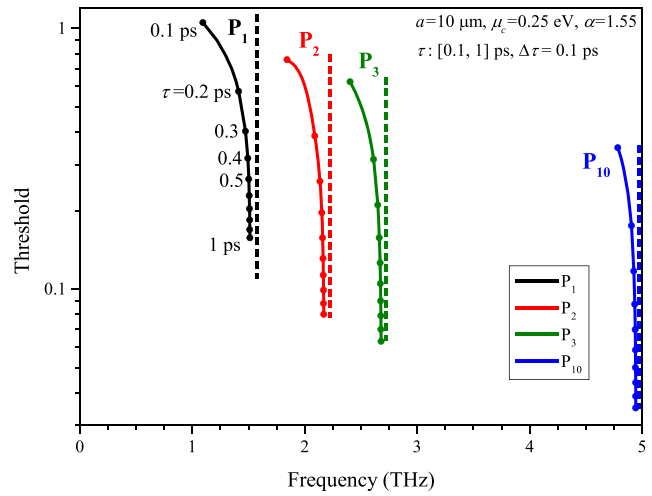


(c)

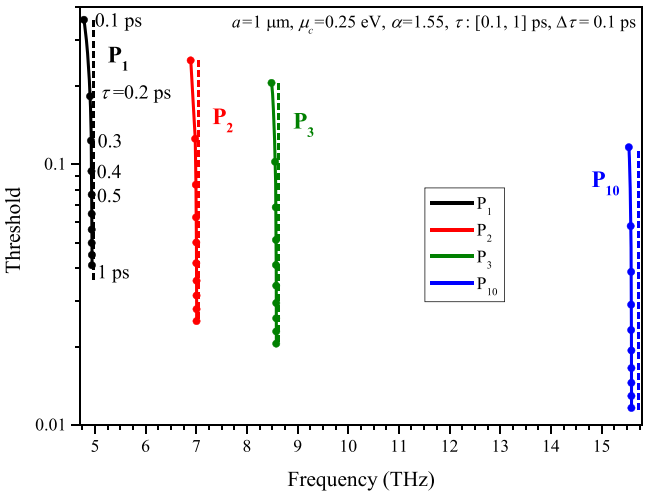
Figure 4. Trajectories of the plasmon modes P_m and wire modes H_{nm} of the single-wire laser with parameters $a = 50 \mu\text{m}$ (a), $10 \mu\text{m}$ (b) and $1 \mu\text{m}$ (c), under the variation of the chemical potential of graphene. Other parameters are as marked.



(a)



(b)



(c)

Figure 5. Trajectories of the plasmon modes P_m and wire modes H_{nm} of the single-wire laser with parameters $a = 50 \mu\text{m}$ (a), $10 \mu\text{m}$ (b) and $1 \mu\text{m}$ (c), under the variation of the electron relaxation time. Other parameters are as marked.

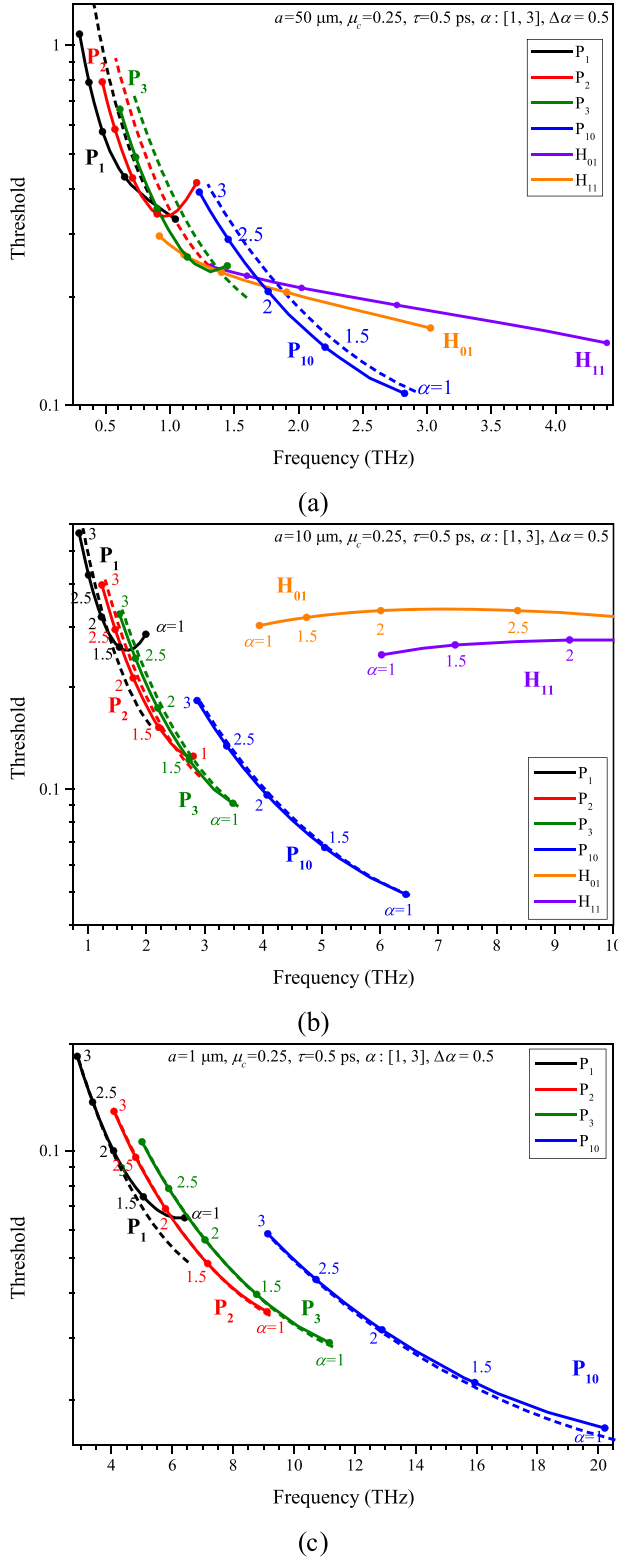


Figure 6. Trajectories of plasmon modes P_m and wire modes H_{nm} of the single-wire laser with radii $a = 50 \mu\text{m}$ (a), $10 \mu\text{m}$ (b) and $1 \mu\text{m}$ (c), under the variation of the refractive index of QW. Other parameters are as marked.

As one can see, only the plasmon-mode frequencies are well tunable using the graphene chemical potential. Making the wire thinner than $10 \mu\text{m}$ shifts QW modes far to the blue side

of spectrum. The larger the τ , the lower the thresholds of all modes; note that if τ varies from realistic 1 ps to fantastic $10 \mu\text{s}$ (see figure 5(a)), then the P_1 threshold is almost stable that points out to the possible radiation loss level. Again, the approximations of (12) and (13), given by the dashed curves, are amazingly accurate except of the low-terahertz and higher than 35 THz frequencies.

6. Full-wave determinantal equations of four symmetry classes of dimer supermodes

In the dimer case, all eigenmodes are in fact ‘supermodes,’ built on the modes of each individual circular wire and optically connected in four possible ways dictated by the two-fold symmetry. Hence, supermodes make quartets instead of pairs because each mode of a stand-alone circular wire is doubly degenerate; this degeneracy is lifted when another circular wire appears. Only the supermodes built of axially symmetric modes of each wire make doublets. Each family of supermodes has either the symmetry or the anti-symmetry of its field with respect to each line of symmetry; they can be conveniently denoted as ‘x-even, y-even’ (EE), ‘x-even, y-odd’ (EO), ‘x-odd, y-odd’ (OO), and ‘x-odd, y-even’ (OE). The ‘even/odd’ conditions, respectively, can be expressed as

$$\frac{\partial H_z}{\partial x} = 0 \text{ at } y = 0 \text{ or } \frac{\partial H_z}{\partial y} = 0 \text{ at } x = 0; H_z = 0 \text{ at } y = 0 \text{ or } x = 0. \quad (15)$$

To reduce the dimer LEP to characteristic equations, we follow the works [20, 30] and use the Fourier expansions of the field function in the local polar coordinates, the addition theorems for the cylindrical functions, and the conditions (15). Here, we look for the magnetic field function as

$$H_z = \begin{cases} H_z^{\text{int}(j)}, & r_j \in \#1, j = 1, 2, \\ H_z^{\text{ext}}, & r_j \in \#2, \end{cases} \quad (16)$$

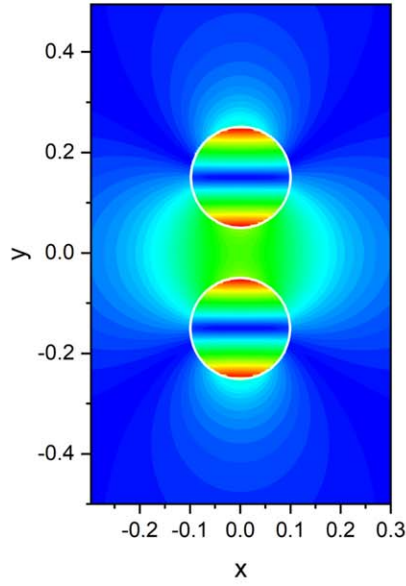
It is convenient to introduce new variables $\psi_j = \phi_j + \pi/2$. Then the internal and external fields, which have the y-even and y-odd symmetry can be expanded as follows:

$$H^{\text{int}(j)}(r, \psi) = \sum_{n=0}^{\infty} y_n^{(j)} J_n(k\alpha r_j) S_n^+(\psi_j), \quad j = 1, 2, \quad (17)$$

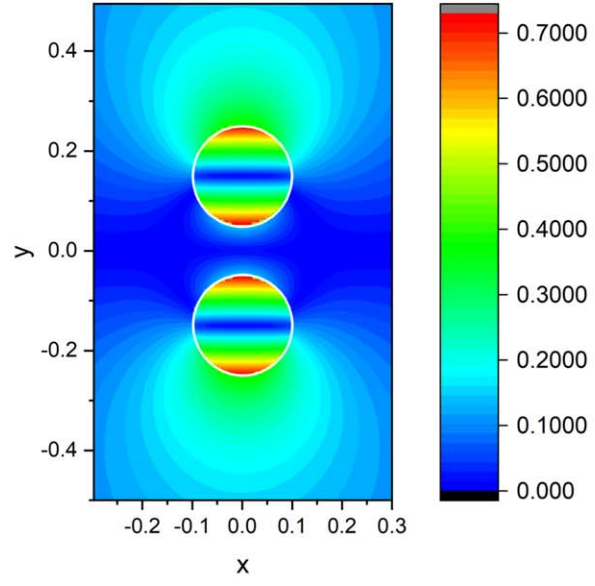
$$H^{\text{ext}}(r, \psi) = \sum_{j=1,2} \sum_{n=0}^{\infty} z_n^{(j)} H_n(kr_j) S_n^{\pm}(\psi_j), \quad (18)$$

where we use the following notations: $S_m^+(\psi) = \cos m\psi$ and $S_m^-(\psi) = \sin m\psi$, $J_n(\cdot)$ and $H_n(\cdot)$ are the Bessel and Hankel (first kind) functions, and $y_n^{(1,2)}$ and $z_n^{(1,2)}$ are unknown coefficients to be found. This representation of the function H satisfies the Helmholtz equation, the Sommerfeld radiation condition, the local power finiteness condition, and the y-even/y-odd symmetry conditions that is (15) at $x = 0$.

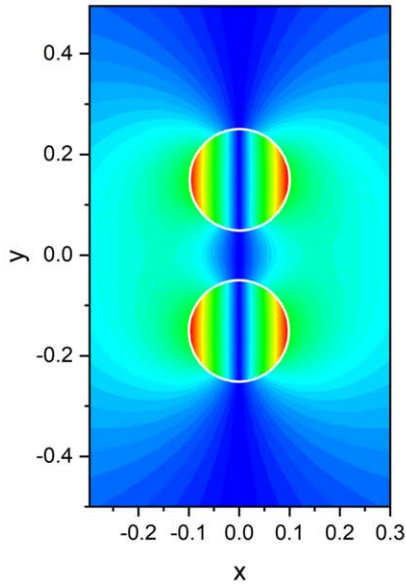
On substituting (17) and (18) into the graphene boundary conditions (1), using the Graph addition theorem for the

EE mode, $a=1 \mu\text{m}$, $s=1 \mu\text{m}$, $\tau=0.5 \text{ ps}$,

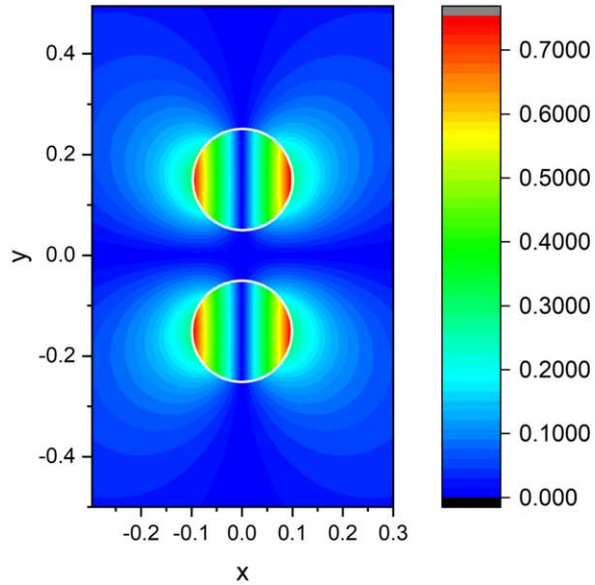
$f=4.56 \text{ THz}$, $\gamma=0.072$
(a)

OE mode, $a=1 \mu\text{m}$, $s=1 \mu\text{m}$, $\tau=0.5 \text{ ps}$, $\alpha=1.55$, $\mu_c=0.2 \text{ eV}$ 

$f=4.55 \text{ THz}$, $\gamma=0.08$
(b)

EO mode, $a=1 \mu\text{m}$, $s=1 \mu\text{m}$, $\tau=0.5 \text{ ps}$,

$f=4.25 \text{ THz}$, $\gamma=0.1$
(c)

OO mode, $a=1 \mu\text{m}$, $s=1 \mu\text{m}$, $\tau=0.5 \text{ ps}$, $\alpha=1.55$, $\mu_c=0.2 \text{ eV}$ 

$f=4.26 \text{ THz}$, $\gamma=0.089$
(d)

Figure 7. The near magnetic field patterns of four supermodes P_1 of the EE (a), OE (b), EO (c), and OO (d) symmetry classes. The threshold values of the frequency of emission and the gain index are marked below each picture.

Hankel functions, and introducing the notations,

$$I = \{\delta_{mn}\}_{m,n=0(1)}^{\infty}, A^{E/O,E(O)} = \{A_{mn}^{E/O,E(O)}\}_{m,n=0(1)}^{\infty}, \quad (19)$$

$$X_{1,2}^{E/O,E(O)} = \{x_n^{(1,2)}\}_{n=0(1)}^{\infty}, \quad (20)$$

$$x_n^{(1,2)} = z_n^{(1,2)} w_n^{-1}, w_n = n!(2/ka)^n \quad (21)$$

where δ_{mn} is the Kronecker symbol, we exclude the unknowns

$X_2^{(pq)}$ because from (15) it follows that

$$X_1^{E/O,E} = \pm X_2^{E/O,E}, X_1^{E/O,O} = \mp X_2^{E/O,O} \quad (22)$$

and obtain the following four matrix equations for $X_1^{(pq)}$:
 x -even/ y -even (EE) and x -odd/ y -even (OE) mode classes

$$(I + A^{E/O,E})X_1^{E/O,E} = 0, \quad (23)$$

$$A_{mn}^{E/O,E} = \pm \mu_n V_m w_m^{-1} D_m^{-1} \times [H_{n-m}(kL)i^{m-n} + H_{n+m}(kL)i^{-m+n}], \quad (24)$$

and x -even/ y -odd (EO) and x -odd/ y -odd (OO) mode classes

$$(I + A^{E/O,O})X_1^{E/O,O} = 0, \quad (25)$$

$$A_{mn}^{E/O,O} = \mp V_m w_m^{-1} D_m^{-1} \times [H_{n-m}(kL)i^{m-n} - (-1)^m H_{n+m}(kL)i^{m+n}], \quad (26)$$

where D_m is given by (6), $\mu_0 = 1/2$, $\mu_{n>0} = 1$ and

$$V_m = J'_m(ka)J'_m(kva) - iZ[\nu J'_m(ka)J_m(kva) - J_m(ka)J'_m(kva)]. \quad (27)$$

The large-index asymptotics of the cylindrical functions allow to establish that each of equations (23) and (25) is a Fredholm second kind matrix equation in the space of sequences $l_2 \otimes l_2$. Thanks to this, their infinite-dimension determinants exist as functions of all parameters of the problem. Besides, thanks to the Fredholm theorems generalized for the operators [38], the characteristic numbers of (23) and (25) are discrete on the plane (k, γ) and depend continuously on the geometrical and material parameters of the problem. Moreover, this guarantees that the approximate characteristic numbers, found from the truncated determinantal equations,

$$\text{Det} \{ \delta_{mn} - A_{mn}^{(p,q)}(k, \gamma) \}_{m,n=0(1)}^N = 0, \quad p, q, = E, O, \quad (28)$$

converge to the exact values for progressively larger truncation numbers N [39]. Note that the matrix elements need no numerical integrations, and hence can be easily computed with machine precision. It should be emphasized that the scaling of the unknowns with the aid of the weight w_n (21) is crucially important. Without this scaling, the matrix elements would decay with $n \rightarrow \infty$ however grow up exponentially with $m \rightarrow \infty$ that prohibits, mathematically, the truncation of the matrix.

7. Dimer-wire laser mode properties

In this section, we present the full-wave numerical data on the lasing frequencies and thresholds of the supermodes of the dimer laser built of two identical graphene-covered QWs.

To illustrate the splitting of the dimer plasmon modes into quartets, we present in figure 7 the near magnetic field patterns of four supermodes P_1 of the EE, OE, EO and OO symmetry classes. Note that the symmetry (antisymmetry) of the H -field entails antisymmetry (symmetry) of the E -field pattern.

In figure 8, we show the trajectories of the dimer plasmon supermode quartets on the plane (f, γ) , under the variation of the chemical potential of graphene. Here, two supermode quartets are present, built on the plasmon modes P_1 and P_2 in each wire, for two values of the inter-wire separation, 100 nm for panel (a) and 1 μm for panel (b). Although being split here, supermode trajectories, in general, are still close to the hyperbola defined by equation (14). Only the ‘dipole’ supermodes $P_1^{(p,q)}$ display deviations, which become smaller if the separation gets larger.

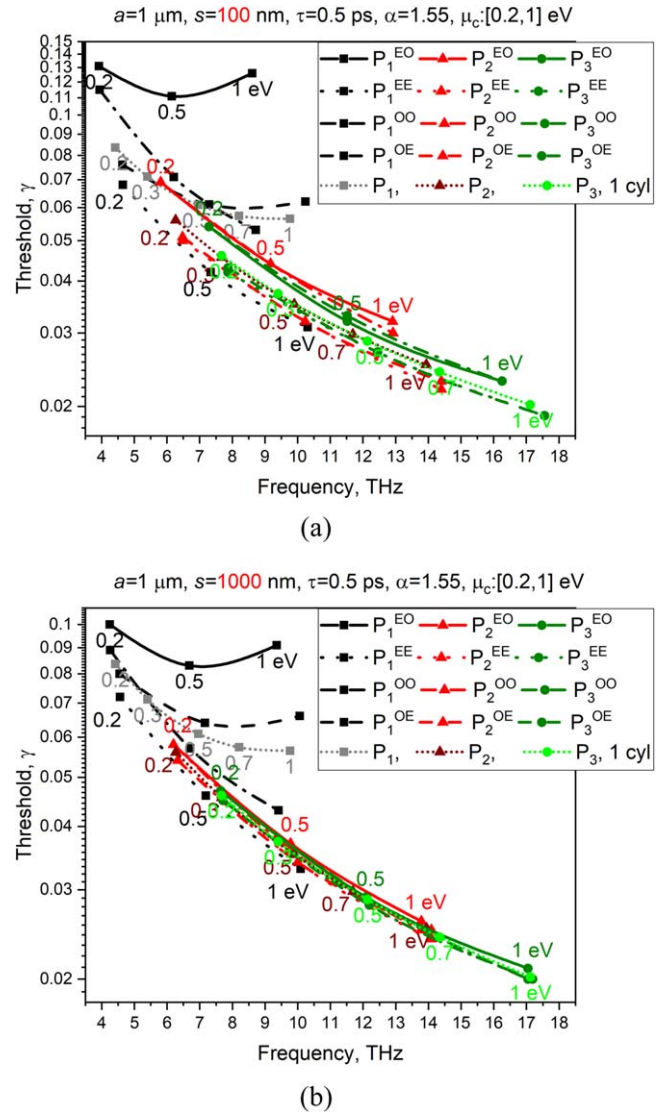


Figure 8. Trajectories of the plasmon supermodes P_m of the dimer-wire laser with parameters $a = 1 \mu\text{m}$ and separation distances $s = 100 \text{ nm}$ (a) and $1 \mu\text{m}$ (b), under the variation of the chemical potential of graphene. Other parameters are as marked.

Finally, in figure 9 we present the mode trajectories of three supermode quartets, $P_{1,2,3}^{(p,q)}$, under the variation of the inter-wire separation distance from 10 nm to 1 μm , for two values of the chemical potential, 0.2 eV for panel (a) and 0.5 eV for panel (b). As expected, if the wires move away from each other, then all four modes of a quartet migrate to the same ‘destination point,’ which is the single-wire mode frequency and threshold (marked with stars). The largest splits and the slowest pace of reaching the limit are again associated with the ‘dipole’ supermodes, $P_1^{(p,q)}$. This can be explained by the fact that the compression of the plasmon-mode fields to the graphene shell increases with the mode index, m , therefore the distance needed for efficient coupling gets smaller. Note that, in all examples, the supermodes built on the wire modes, H_{01} and H_{11} , are off the studied range of frequencies, from the blue side.

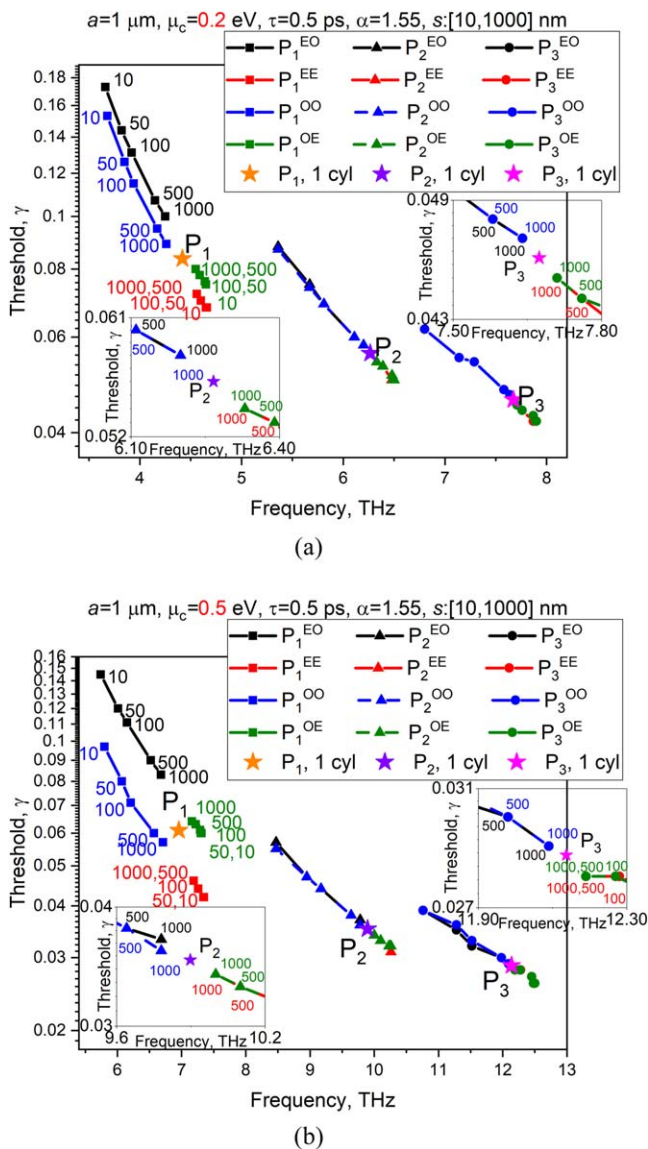


Figure 9. Trajectories of the plasmon supermodes P_m of the dimer-wire laser with parameters $a = 1 \mu\text{m}$ and the chemical potential of graphene $\mu_c = 0.2 \text{ eV}$ (a) and 0.5 eV (b), under the variation of the inter-wire separation, s . Other parameters are as marked.

8. Conclusions

We have presented the computational electromagnetic analysis of the plasmonic graphene nanolasers based on the circular QW wrapped in graphene and a dimer of such wires. Using the Kubo formalism and separation of variables, adapted to the LEP approach, we have derived full-wave transcendental and determinantal equations for the transversal mode emission frequencies and the material gain thresholds in the single wire and dimer cases, respectively. These equations are easily coded in straightforward manner and computed with machine precision, making the use of commercial codes unnecessary.

Besides, for a single-wire laser we have derived approximate analytical expressions for the plasmon-mode

frequencies and thresholds, neglecting the radiation losses and only using the Drude term (i.e. the intraband component) in the description of graphene's surface conductivity. These expressions are in excellent agreement with full-wave computations in very wide range of the wire radii and frequencies. As new result, we have found that the product of the plasmon-mode frequencies and thresholds is close to a constant, defined by the QW refractive index and electron relaxation time, only.

If the QW radius is smaller than $10 \mu\text{m}$, then the plasmon modes or supermodes have lower frequencies and thresholds than the 'parasitic' QW modes however in thicker wires they can be similar. As expected, only the plasmon-mode characteristics can be well controlled with the aid of the graphene chemical potential. In the dimer, the plasmon supermodes form tight quartets, approaching the single-wire mode characteristics if the inter-wire separation becomes comparable to the radius. Whatever the separation, the EE supermode, featuring the x -even and y -even H-field, shows the threshold, lower than of the same mode in a single graphene-covered QW. This can be explained by the fact that this supermode has zero E field at the x and y axes. We believe that these results bring a clearer vision of how to build single-mode graphene-covered plasmonic nanolasers and their arrays.

Acknowledgments

Authors wish to thank the National Research Foundation of Ukraine for support via grant #2020-02-0150. DOH and SVD are grateful to the University of Rennes 1 for hospitality and the PAUSE Program of the Solidarity with Ukraine of the Ministry of Higher Education, Research and Innovations, France for the emergency support in 2022. AIN is grateful to Politecnico di Torino for hospitality and the Ministry of Universities and Research, Italy for the emergency support in 2022.

Data availability statement

All data that support the findings of this study are included within the article (and any supplementary files).

ORCID iDs

Dariia O Herasymova <https://orcid.org/0000-0001-6569-1226>

Sergii V Dukhopelnykov <https://orcid.org/0000-0002-0639-988X>

Denys M Natarov <https://orcid.org/0000-0003-4170-9211>

Tatiana L Zinenko <https://orcid.org/0000-0002-7218-1344>

Mario Lucido <https://orcid.org/0000-0001-8661-5601>

Alexander I Nosich <https://orcid.org/0000-0002-3446-8168>

References

- [1] Geim A K and Novoselov K S 2007 The rise of graphene *Nat. Mater.* **6** 183–91
- [2] Hanson G W 2008 Dyadic Green's functions and guided surface waves for a surface conductivity model of graphene *J. Appl. Phys.* **103** 064302
- [3] Low T and Avouris P 2014 Graphene plasmonics for terahertz to mid-infrared applications *ACS Nano* **8** 1086–101
- [4] Ullah Z et al 2020 A review on the development of tunable graphene nanoantennas for terahertz optoelectronic and plasmonic applications *Sensors* **20** 1401
- [5] Fallahi A and Perruisseau-Carrier J 2012 Design of tunable biperiodic graphene metasurfaces *Phys. Rev. B* **86** 195408
- [6] Zinenko T L, Matsushima A and Nosich A I 2017 Surface-plasmon, grating-mode and slab-mode resonances in THz wave scattering by a graphene strip grating embedded into a dielectric slab *IEEE J. Sel. Top. Quant. Electron.* **23** 4601809
- [7] Oguzer T, Altintas A and Nosich A I 2017 Focusing of THz waves with a microsize cylindrical reflector made of graphene in the free space *J. Eur. Opt. Soc.* **13** 16
- [8] Kaliberda M E et al 2019 Diffraction of the H-polarized plane wave by a finite layered graphene strip grating *Int. J. Microwave Wireless Technol.* **11** 326–33
- [9] Yevtushenko F O et al 2021 Electromagnetic characterisation of tuneable graphene-strips-on-substrate metasurface in the whole THz range: analytical regularization and interplay of natural-mode resonances *IET Microw., Antennas Propagat.* **15** 1225–39
- [10] Apalkov V and Stockman M I 2014 Proposed graphene nanospaser *Light: Sci. Appl.* **3** e191
- [11] Liu B et al 2017 Open resonator electric spaser *ACS Nano* **1** 12573–82
- [12] Ning C-Z 2021 Spaser or plasmonic nanolaser? Reminiscences of discussions and arguments with Mark Stockman *Nanophotonics* **10** 3619–22
- [13] Dai C, Agarwal K, Bechtel H A, Liu C, Joung D, Nemilentsau A, Su Q, Low T, Koester S J and Cho J-H 2021 Hybridized radial and edge coupled 3D plasmon modes in self-assembled graphene nanocylinders *Small* **17** 2100079
- [14] Zhu B, Ren G, Yang Y, Gao Y, Wu B, Lian Y and Wang J 2015 Field enhancement and gradient force in the graphene-coated nanowire pairs *Plasmonics* **10** 839–45
- [15] Naserpour M, Zapata-Rodríguez C J, Vuković S M, Pashaieadi H and Belić M R 2017 Tunable invisibility cloaking by using isolated graphene-coated nanowires and dimers *Sci. Rep.* **7** 1–14
- [16] Velichko E A 2016 Evaluation of a dielectric microtube with a graphene cover as a refractive-index sensor in the THz range *J. Opt.* **18** 035008
- [17] Cuevas M et al 2016 Complex frequencies and field distributions of localized surface plasmon modes in graphene-coated subwavelength wires *J. Quant. Spectr. Rad. Transfer* **173** 26–33
- [18] Cuevas M et al 2020 Coupled plasmonic graphene wires: theoretical study including complex frequencies and field distributions of bright and dark surface plasmons *J. Opt. Soc. Am. B* **37** 3084–93
- [19] Dukhopelnikov S V et al 2021 Circular dielectric rod with conformal strip of graphene as tunable terahertz antenna: interplay of inverse electromagnetic jet, whispering gallery and plasmon effects *IEEE J. Sel. Top. Quant. Electron.* **27** 4600908
- [20] Herasymova D O, Dukhopelnikov S V and Nosich A I 2021 Infrared diffraction radiation from twin circular dielectric rods covered with graphene: plasmon resonances and beam position sensing *J. Opt. Soc. Am. B* **38** C183–90
- [21] Prelat L et al 2021 Spaser and optical amplification conditions in graphene-coated active wires *J. Opt. Soc. Am. B* **38** 2118–26
- [22] Smotrova E I et al 2011 Optical theorem helps understand thresholds of lasing in microcavities with active regions *IEEE J. Quant. Electron.* **47** 20–30
- [23] Byelobrov V O et al 2010 Low-threshold lasing eigenmodes of an infinite periodic chain of quantum wires *Opt. Lett.* **35** 3634–6
- [24] Smotrova E I et al 2013 Spectra, thresholds and modal fields of a kite-shaped microcavity laser *J. Opt. Soc. Am. B* **30** 1732–42
- [25] Spiridonov A O et al 2019 Why elliptic microcavity lasers emit light on bow-tie-like modes instead of whispering-gallery-like modes *Opt. Commun.* **439** 112–7
- [26] Shapoval O V et al 2017 Electromagnetic engineering of a single-mode nanolaser on a metal plasmonic strip placed into a circular quantum wire *IEEE J. Sel. Top. Quant. Electron.* **23** 1501609
- [27] Natarov D M et al 2019 Electromagnetic analysis of the lasing thresholds of hybrid plasmon modes of a silver tube nanolaser with active core and active shell *Beilstein J. Nanotechnol.* **10** 294–304
- [28] Spiridonov A O et al 2020 Mathematical and numerical analysis of the generalized complex-frequency eigenvalue problem for two-dimensional optical microcavities *SIAM J. Appl. Math.* **80** 1977–98
- [29] Natarov D M, Natarova A O and Zinenko T L 2021 Frequencies and thresholds of transversal plasmon modes of the laser shaped as a circular quantum wire wrapped in graphene cover *Proc. IEEE Ukrainian Conf. Electrical Computer Eng. (UKRCON-2021), Lviv* pp 177–180
- [30] Herasymova D O, Dukhopelnikov S V and Zinenko T L 2021 Electromagnetic eigenvalue problem for twin dielectric rods covered with graphene: symmetry classes of the H-polarized supermodes *Proc. IEEE Ukrainian Conf. Electr. Comp. Eng. (UKRCON-2021), Lviv* pp 92–95
- [31] Nojima S 2005 Theoretical analysis of feedback mechanisms of two-dimensional finite-sized photonic-crystal lasers *J. Appl. Phys.* **98** 043102
- [32] Mock A 2010 First principles derivation of microcavity semiconductor laser threshold condition and its application to FDTD active cavity modeling *J. Opt. Soc. Am. B* **27** 2262–72
- [33] Chang S W 2012 Confinement factors and modal volumes of micro- and nanocavities invariant to integration regions *IEEE J. Sel. Top. Quant. Electron.* **18** 1771–80
- [34] Huang Y and Lu Y Y 2014 Efficient method for lasing eigenvalue problems of periodic structures *J. Mod. Opt.* **61** 390–6
- [35] Yu H-Q, Jiang S-M and Wu D-J 2015 Efficient surface plasmon amplification in gain-assisted silver nanotubes and associated dimers *J. Appl. Phys.* **117** 153101
- [36] Velichko E A and Natarov D M 2018 Localized versus delocalized surface plasmons: dual nature of resonances on a silver circular wire and a silver tube of large diameter *J. Opt.* **20** 075002
- [37] Dukhopelnikov S V et al 2020 Integral equation analysis of terahertz backscattering from circular dielectric rod with partial graphene cover *IEEE J. Quant. Electron.* **56** 8500208
- [38] Steinberg S 1968 Meromorphic families of compact operators *Arch. Rat. Mech. Anal.* **31** 372–9
- [39] Karma O 1996 Approximation in eigenvalue problems for holomorphic Fredholm operator function. II. Convergence rate *Numer. Funct. Anal. Optim.* **17** 389–408